Applied Catalysis B: Environmental 330 (2023) 122644

Contents lists available at ScienceDirect

Applied Catalysis B: Environmental

journal homepage: www.elsevier.com/locate/apcatb

Enhanced ammonia decomposition activity over unsupported Co_3O_4: Unravelling the promotion effect of alkali metal

Wenshuo Zhang [a,b,*], Weili Zhou [a], Yangfeng Li [a], Jie Ren [c], Zhandong Wang [a,d,e,*]

[a] National Synchrotron Radiation Laboratory, University of Science and Technology of China, Hefei 230029, PR China
[b] College of Pharmacy and Chemistry & Chemical Engineering, Taizhou University, Taizhou 225300, PR China
[c] Department of Thermal Science and Energy Engineering, University of Science and Technology of China, Hefei 230026, PR China
[d] State Key Laboratory of Fire Science, University of Science and Technology of China, Hefei 230026, PR China
[e] Dalian National Laboratory for Clean Energy, Dalian 116023, PR China

ARTICLE INFO

Keywords:
Ammonia decomposition
Carbon-free hydrogen production
Cobalt-based catalysts
Alkali promoter

ABSTRACT

To deeply understand the effect of alkali metals on the structure-activity relationship of cobalt-based catalysts for ammonia decomposition, unsupported Co_3O_4 was fabricated as catalyst model. It was found that alkali metals (Na and K) enhanced the NH_3 decomposition performance of Co_3O_4 significantly, with NH_3 conversion even higher than supported ones. As indicated by characterizations, appropriate amount of Na doping generated more reducible Co^{3+}, which induced strong interaction with NH_3 during reaction. As a result, it was easier for NH_3 as well as -NH_2 intermediate to dehydrogenate at low temperature. Therefore, the intrinsic activity of Co_3O_4 for NH_3 decomposition was increased. This study not only provided a novel strategy in the practical use of cobalt-based catalysts for NH_3 decomposition, but also gave deep insight into the promotion effect of alkali metal.

1. Introduction

The utilization of hydrogen, which has been recognized as ideal clean and renewable energy, is restricted by disadvantages in storage and transportation due to its low energy density and boiling point [1,2]. As an alternative carbon-free hydrogen carrier, liquid ammonia has raised attention due to high H_2 content (17.8 % by weight), low production cost, as well as the established storage and distribution infrastructure [3–5]. Catalytically decomposition of NH_3 to H_2 using efficient catalysts provides a viable approach to the utilization of NH_3 as a hydrogen carrier, for instance, the in-situ H_2 production by fuel cells [6–8]. As a result, it is urgent to design efficient catalysts for the production of carbon-free H_2 by cracking NH_3.

For decades, extensive studies focused on the higher conversion of NH_3 decomposition at low temperature (below 500 °C), in which Ru-based catalysts were reported to be the most effective [2,9–13]. Nonetheless, the scarcity and expensiveness of noble metals hamper the commercialization of Ru-based catalysts. In this case, non-noble transition metals (Ni, Co, Fe, et al.) with low price are promising candidates and have been widely studied for NH_3 decomposition as well [14–17]. Among these transition metals, much effort has been focused on the design of cobalt-based catalysts with relatively high intrinsic activity, by means of the fabrication and modification of supports [18–21] or effect of promoters [22,23]. Alkali metals (Li, K, Cs, et al.) are widely accepted as basic promoters for NH_3 decomposition catalysts, which benefited the desorption of products [24,25]. As for supported cobalt-based catalysts, addition of K was found to modify the electronic structure and basicity, and thus improve the low-temperature catalytic activity [22,23]. However, due to the complication by various supports, the effect of alkali metals on the real active site remains unclear.

Compared with supported ones, pure Co_3O_4 showed poor activity for the decomposition of NH_3 mainly due to the low specific surface area [20,26,27]. However, according to previous research, unsupported Co catalysts exhibited high NH_3 decomposition activity when coupling with other metals, including Re, Mo, Fe, Sm [16,28–31]. Moreover, unsupported Co_3O_4 has relatively simple structure and provide advantage to discriminate the real active phase as well as the promotion effect of additives without the complication by metal-support interaction. As for other catalytic reactions (for instance, soot combustion and toluene oxidation), alkali metals (K, Na) were found to have an influence on the valence state of Co, and thus benefited the catalytic activity of Co_3O_4 [32,33]. Nevertheless, as for NH_3 decomposition reaction, whether alkali metals play a role in the catalytic performance of Co_3O_4 has not been systematically investigated. Furthermore, alkali hydroxides

* Corresponding authors at: National Synchrotron Radiation Laboratory, University of Science and Technology of China, Hefei 230029, PR China.
E-mail addresses: wenshuozhang@ustc.edu.cn (W. Zhang), zhdwang@ustc.edu.cn (Z. Wang).

https://doi.org/10.1016/j.apcatb.2023.122644
Received 22 January 2023; Received in revised form 12 March 2023; Accepted 14 March 2023
Available online 15 March 2023

(NaOH, KOH, et al.) are common-used precipitants and structure-directing agents in the preparation process, which can easily introduce alkali metals into catalysts. Hence, it is valuable to study the effect of alkali metals on the NH_3 decomposition activity of Co_3O_4.

In this work, Na-doped Co_3O_4 samples were prepared in a simple precipitation method, in which NaOH worked as both precipitant and additive. It was found that even small variation in the amount of Na has an obvious effect on the low-temperature activity of Co_3O_4. Further characterizations were carried out on both fresh and used samples to study the promotion effect intensively. Unexpectedly, besides the influence of Na on the surface basicity, which is already widely-accepted, the presence of Na also modified the reducibility of Co, and thus promoting the stepwise dehydrogenation of NH_3. This work illustrated the non-negligible influence of alkali metal on cobalt-based catalysts for NH_3 decomposition, along with deep understanding of the influence of alkali additives on the NH_3 cracking ability of cobalt-based catalysts.

2. Materials and methods

2.1. Catalyst preparation

Typically, 5.821 g $Co(NO_3)_3{\cdot}6H_2O$ was dissolved in 100 mL ultrapure water. Then, a certain amount of NaOH (1 mol L^{-1}) was added dropwise into the aforementioned solution until pH = 9 with continuous stirring. After stirring for 1 h, the solution was ageing for another 3 h. The obtained precipitates were filtered and washed using 200 mL, 400 mL, 600 mL ultrapure water, respectively. The synthesized samples were then dried overnight at 105 °C and calcined at 600 °C in air for 3 h. Depending on the Na contents calculated by inductively coupled plasma optical emission spectrometer (ICP-OES) experiments (Table S1), the samples were labelled as 1.22 %Na-Co_3O_4, 0.88 %Na-Co_3O_4, 0.77 %Na-Co_3O_4, respectively. In addition, the sample which was directly filtered without further washing was noted as Na-Co_3O_4-unwashed. For comparison, pure Co_3O_4 was prepared by citric acid method. Briefly, 5.821 g $Co(NO_3)_3{\cdot}6H_2O$ and 5.044 g citric acid were dissolved in 20 mL ultrapure water and stirred until totally drying. The obtained solid was dried overnight at 105 °C, grinded to powder and calcined at 600 °C for 3 h in air.

2.2. Activity test

Ammonia decomposition measurements were carried out in a fixed-bed quartz tube at atmosphere pressure. Each sample (100 mg, 40–60 mesh) was tested with a gas hourly space velocity (GHSV) of 30,000 mL g_{cat}^{-1} h^{-1}. Prior to tests, the catalysts were reduced in 15 % NH_3 (50 mL min^{-1}) at 500 °C for 1 h, followed by cooling to 400 °C under Ar flow. Finally, the reactions were carried out in the range of 400–600 °C (at intervals of 50 °C) with feed gas consisted of 15 % NH_3 balanced by Ar. During the test, the catalysts were exposed to each temperature for 50 min

The gas composition was analyzed using an online gas chromatograph equipped with a Porapak-Q column and a thermal conductivity detector. The NH_3 conversions were calculated as follow.

$$NH_3\text{conversion}(\%) = \left(1 - \frac{[NH_3]_{out}}{[NH_3]_{in}}\right) \times 100\% \quad (1)$$

where $[NH_3]_{in}$ and $[NH_3]_{out}$ stand for the concentrations of NH_3 fed into and flowing out of the reactor.

2.3. Kinetic studies

The apparent activation energy (E_a) for NH_3 decomposition was measured in the same reactor as activity tests. The feed gas composition was the same as activity tests. In this case, the conversion of NH_3 was controlled below 20 %.

The reaction rate of NH_3 conversion normalized by specific surface area was calculated as follows:

$$-R_{NH3} = \frac{F_{NH3} \times X_{NH3}}{W \times S} \quad (2)$$

where F_{NH3} is the molar flow rate of NH_3, X_{NH3} is the conversion of NH_3, W is the weight of catalyst and S is the specific surface area.

2.4. Catalyst characterization

N_2-physisorption analysis was performed at 77 K using a Micromeritics ASAP 2460. Prior to analysis, each sample was degassed at 300 °C for 3 h. The specific surface areas were calculated by the BET (Brunauer-Emmett-Teller) equation in the 0.05–0.30 partial pressure range. X-ray diffraction (XRD) patterns were obtained using a Rigaku SmartLab rotating-anode X-ray diffractometer. The scan range of 2θ was from 10° to 80° with a step size of 0.02°. Raman spectra were recorded on a Horiba LabRAM HR Evolution using a 532 nm laser beam as the excitation source for the measurement. The X-ray absorption fine structure (XAFS) measurements, including X-ray absorption near-edge structure (XANES) and extended X-ray absorption fine structure (EXAFS), were carried out at room temperature on a Table-XAFS-500A in Specreation Instrument Co., Ltd. in Hefei, China. The spectra were analyzed (background subtraction, normalization, and Fourier transform) using Athena.

XPS measurements were carried out on an X-ray photoelectron spectrometer (Kratos Axis supra+) with Al Ka radiation (1486.6 eV). The binding energies of Co 2p, O 1 s, Na 1 s, and N 1 s were calibrated using the C 1 s peak (BE = 284.8 eV) as the standard. The temperature-programmed reduction with hydrogen (H_2-TPR) experiments were carried out on a Micromeritics Auto Chem 2920 chemisorption analyzer. In a typical measurement, 100 mg of sample was first preprocessed in a flow of N_2 with a total flow rate of 50 mL min^{-1} at 300 °C for 1 h and then cooled to 50 °C, followed by Ar/He purging for 1 h. Then, the temperature was linearly increased from 50° to 800°C at a heating rate of 10 °C min^{-1} in a flow of 10 vol % H_2/Ar (50 mL min^{-1}), during which the H_2 consumption was continuously recorded by a thermal conductivity detector (TCD).

The CO_2-TPD and NH_3-TPD experiments were also performed on Micromeritics Auto Chem 2920 chemisorption analyzer. Typically, 100 mg of sample was first preprocessed in a flow of H_2/Ar with a total flow rate of 30 mL min^{-1} at 500 °C for 1 h and then cooled to 50 °C, followed by Ar/He purging for 0.5 h. The samples were then exposed to a flow of 10 % CO_2/Ar (30 mL min^{-1}) at 50 °C for 1 h, followed by Ar/He purging for 0.5 h. The temperature was first raised to 100 °C and remained 1 h, and finally elevated to 600 °C linearly at a rate of 10 °C min^{-1}. The desorption of CO_2 was recorded by TCD. For NH_3-TPD experiments, 100 mg of sample was first preprocessed in a flow of 5 % NH_3/He with a total flow rate of 50 mL min^{-1} at 500 °C for 1 h and then cooled to 50 °C, followed by He purging. The samples were then exposed to a flow of 5 % NH_3/He (50 mL min^{-1}) at 50 °C for 1 h, followed by He purging for 1 h. The temperature was elevated to 600 °C linearly at a rate of 10 °C min^{-1}. The desorption of NH_3 was recorded by TCD. For NH_3 temperature programmed surface reaction (NH_3-TPSR) experiment, 100 mg of sample (30–40 mesh) was first pretreated in a flow of 5 % NH_3/Ar with a total flow rate of 100 mL min^{-1} at 500 °C for 1 h and then cooled to 50 °C, followed by Ar purging for 1 h. The samples were then exposed to 5 % NH_3/Ar (100 mL min^{-1}) with the temperature elevated to 600 °C linearly at a rate of 5 °C min^{-1}. The products (H_2 and N_2) and unreacted NH_3 were continuously pumped and analyzed by synchrotron VUV photoionization mass spectrometry (SVUV-PIMS) using a beamline at the Atomic & Molecular Physics Beamline (BL09U) of the National Synchrotron Radiation Laboratory in Hefei, China.

The Diffuse Reflectance Infrared Fourier Transform (DRIFT) experiments were performed on an FTIR spectrometer (Nicolet IS50) equipped

with MCT/A detector cooled by liquid nitrogen. The background spectra were collected in flowing Ar and automatically subtracted. All the spectra were recorded by accumulating 32 scans with a resolution of 4 cm^{-1}. Prior to the experiment, each sample was pretreated in Ar at 400 °C for 1 h. Adsorption and reaction condition: 1 % NH_3/Ar (50 mL min^{-1}) with Ar purge (50 mL min^{-1}) when needed.

3. Results and discussion

To evaluate the effect of Na on the NH_3 decomposition performance of Co_3O_4, the catalytic activity of all the prepared samples was tested with results shown in Fig. 1a. It is observed that pure Co_3O_4 without Na addition (Co_3O_4-CA) exhibited the lowest catalytic performance among all tested samples, with the NH_3 conversion of only 76 % at even 600 °C. In contrast, Co_3O_4 with 0.77 % Na addition generated obviously higher NH_3 conversion with the value over 90 % at 600 °C, which indicated the promotion effect of small amount of Na. Among all the Na-doped samples, 1.22 %Na-Co_3O_4 showed the highest NH_3 conversion with the value of 97 % at 550 °C. The difference in the catalytic performance of Na-doped samples revealed that even small variation in Na content had an influence on the activity for cracking NH_3.

To further illustrate the effect of Na on the catalytic activity of Co_3O_4, Arrhenius plots for the reaction rates of NH_3 decomposition were measured over the prepared samples. The values of activation energy (E_a) and pre-exponential factor (A) of each sample were calculated from the Arrhenius plots (Table S2). As shown in Fig. 1b, the activation energy of 1.22 %Na-Co_3O_4 (with the value of 90.1 kJ mol^{-1}) was clearly lower than other samples, which was in good accordance with its higher catalytic activity. This further confirmed the promotion effect of Na on the NH_3 decomposition activity of cobalt-based catalysts. Interestingly, it is also noted that the pre-exponential factor of 1.22 %Na-Co_3O_4 was the lowest (lower by 1–4 orders of magnitude than other Na-doped samples and Co_3O_4-CA), which indicated fewer active sites. This result revealed that moderate addition of Na (1.22 %) increased the intrinsic activity of per active site over Co_3O_4, which agreed well with the higher reaction rate of 1.22 %Na-Co_3O_4 compared with other samples as shown in Fig. 1b. In a word, it is clear that the amount of Na has a non-negligible effect on the performance of Co_3O_4 for NH_3 cracking, in which 1.22 %Na-Co_3O_4 exhibited the highest intrinsic activity.

Due to the reducing atmosphere at high temperature, the structural property of samples changed during the reaction process [31]. Therefore, the structural property of fresh catalysts, as well as samples after pretreatment and reaction, was characterized. From the results of specific surface area, pore volume, and average pore size in Table S3, it was found that the specific surface area of the three samples were close, with the values around 18 m^2 g^{-1}. The specific surface areas of used samples were lower compared with fresh ones, in which the value of 1.22 % Na-Co_3O_4 was the lowest (6.0 m^2 g^{-1}) among all the Na-doped samples. The results illustrated that specific surface area is not the decisive factor for the difference in catalytic activity. In addition, the specific surface area of Co_3O_4-CA was only 0.16 m^2 g^{-1}, much smaller than samples prepared by precipitation method, which was possibly an important factor for its poor catalytic performance (Fig. 1).

The XRD patterns of fresh 1.22 %Na-Co_3O_4, 0.88 %Na-Co_3O_4, and 0.77 %Na-Co_3O_4 are shown in Fig. 2a, with typical diffraction peaks of Co_3O_4 (the same as Na-Co_3O_4-unwashed and Co_3O_4-CA as shown in Fig. S1a). It should be noted that no peak related to Na was detected, indicating high dispersion of Na over Co_3O_4 [26,34]. Comparing the Co_3O_4 diffraction peaks of the three samples, it was found that the peak intensity gradually decreased with Na doping, which implicated the decreased crystallinity of Co_3O_4 phase. It was also observed that the diffraction peaks of Co_3O_4 were broader over 1.22 %Na-Co_3O_4, implying smaller particle size according to Scherer's equation. This further validated that Na partly inserted into the lattice and inhibited the growth of Co_3O_4 [33,35,36]. It is reasonable that the samples were reduced by NH_3 during the pretreatment and reaction process. Diffraction peaks of metal Co (Co^0), which was considered as active site for NH_3 decomposition [22], were observed over used samples (Fig. S1b and S2a). It is also noted that the intensity of Co^0 diffraction peaks over used 1.22 % Na-Co_3O_4 was much stronger than 0.88 %Na-Co_3O_4 and 0.77 % Na-Co_3O_4 (Fig. S2a), indicative of higher degree of crystallinity.

To investigate the lattice vibrational states of the samples, Raman spectroscopy was applied. As for fresh samples in Fig. 2b, the peaks appeared at 475 cm^{-1} and 682 cm^{-1} were assignable to the E_g and $A_{1\,g}$ modes of Co_3O_4, respectively, together with peaks at 516 cm^{-1} and 613 cm^{-1} which were ascribed to $F_{2\,g}$ mode of Co_3O_4 [14,31,37]. Also, it should be noted that comparing with 0.77 %Na-Co_3O_4, the peaks of 0.88 %Na-Co_3O_4 and 1.22 %Na-Co_3O_4 shifted slightly to lower frequencies. This is possibly attributed to the lattice distortion or residual stress by Na doping [32,33,38]. After reaction, as shown in Fig. S2b, Raman peaks of Co_3O_4 appeared and shifted to higher frequencies compared with fresh ones, which was possibly due to the re-oxidization of surface when exposed to the air [31].

XAFS measurements were conducted to further determine the coordination environment and chemical state of Co. As shown in the XANES spectra in Fig. S3, the adsorption edge position of the three samples were close, which indicated similar mean oxidation state of Co. As indicated in the R space spectrum (Fig. 2c), typical Co_3O_4 structure was revealed with the peak around 1.4 attributed to Co-O bond and those around 2.4 and 3.0 correspond to Co-Co (O_h, octahedral) and Co-Co (T_d,

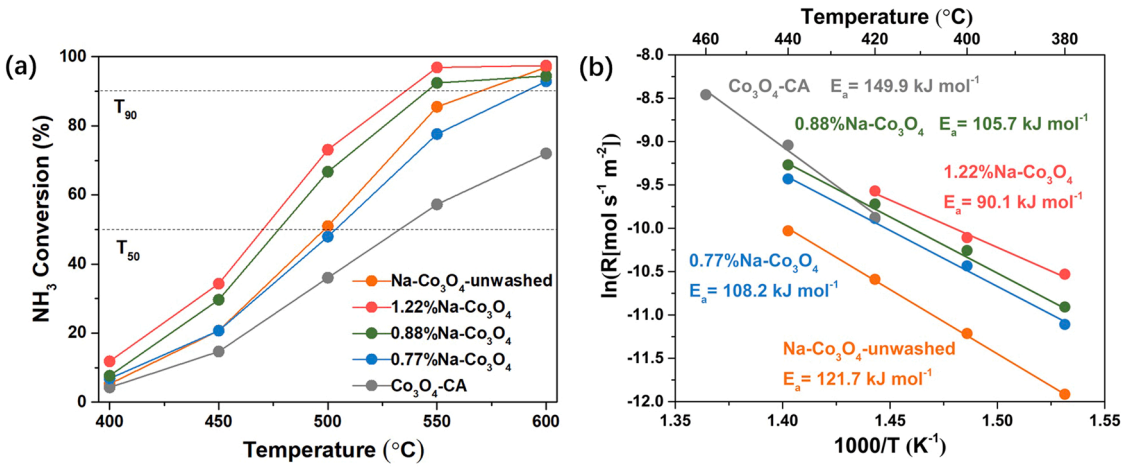

Fig. 1. (a) NH_3 conversion and (b) Arrhenius plots for the reaction rates of NH_3 decomposition over Na-doped Co_3O_4 catalysts and Co_3O_4-CA. GHSV = 30,000 mL g_{cat}^{-1} h^{-1}.

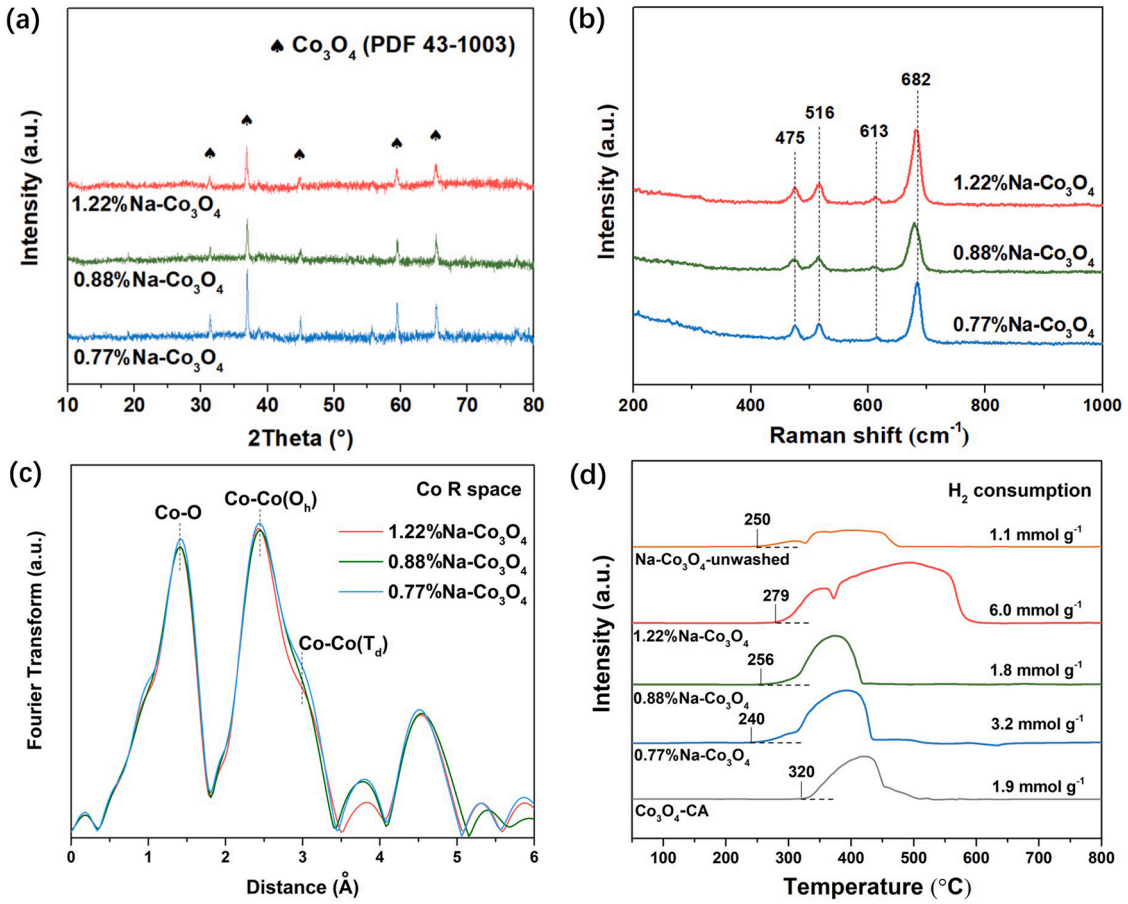

Fig. 2. (a) XRD patterns, (b) Raman results, (c) Fourier-transformed EXAFS spectra of fresh 1.22 %Na-Co_3O_4, 0.88 %Na-Co_3O_4, and 0.77 %Na-Co_3O_4, (d) H_2-TPR results over Na-doped Co_3O_4 catalysts and Co_3O_4-CA.

tetrahedral), respectively [39–41]. Compared with 0.77 %Na-Co_3O_4 and 0.88 %Na-Co_3O_4, the lower peak intensity of 1.22 %Na-Co_3O_4 suggested lower coordination number of Co atoms, which indicated weaker coordination between cobalt and oxygen and was probably related to structural distortion [38,42]. Combined with Raman results, a slightly weaker Co-O coordination of 1.22 %Na-Co_3O_4 compared with 0.77 %Na-Co_3O_4 was confirmed, which was possibly related to the difference in the NH_3 cracking performance.

Furthermore, H_2-TPR experiments were carried out to identify the effect of Na on the redox ability of Co, with results shown in Fig. 2d. As alkali metals are unreducible by hydrogen below 900 °C [36], all the consumption peaks are ascribed to Co species. For all the prepared samples, overlapping reduction peaks were observed, indicating the reduction of Co_3O_4 in two steps: the reduction from Co_3O_4 to CoO, and the reduction from CoO to metal Co at higher temperature [32,33,38]. The reduction of Co over Na-doped samples started between 240 °C and 279 °C, which were much lower than that of Co_3O_4-CA. This result indicated that Na-doped Co_3O_4 accepted more electrons than pure Co_3O_4, which was probably related to the higher reactivity [33]. Considering the two-stage reduction of Co_3O_4, in which the H_2 consumption ratio of the two steps is 1:3 theoretically [38], the H_2-TPR results were further fitted into subpeaks with results shown in Fig. S4. It was noticed that the peak area of the first step (reduction of Co^{3+}) over 1.22 %Na-Co_3O_4 was larger compared with 0.77 %Na-Co_3O_4 and 0.88 %Na-Co_3O_4, which indicated more reducible Co^{3+}. In addition, the largest H_2 consumption amount (6.0 mmol g^{-1}) was observed over 1.22 %Na-Co_3O_4 among all the samples, indictive of the strongest reducibility [43]. It is speculated that the enhanced reducibility of Co over 1.22 %Na-Co_3O_4 may be related to the weaker Co-O coordination of fresh sample, and account for the higher degree of crystallinity of Co^0 for used sample, along with the higher NH_3 cracking activity.

Further investigations focused on the surface property of prepared samples. XPS experiments were carried out to explore the surface elemental compositions and valence states of fresh and used samples. The Co 2p results of all fresh samples are shown in Fig. 3a and Fig. S5a. The peaks observed around 780.1 eV and 795.2 eV were ascribed to Co 2p3/2 and Co 2p1/2, with satellite peaks around 803.5 eV and 788.4 eV [44]. The spin-orbit splitting between the two spin orbits is 15.1 eV, which proves the presence of Co_3O_4 [20,30,45] and is in consistence with XRD and Raman results. Furthermore, the Co 2p3/2 and Co 2p1/2 peaks were deconvoluted into two peaks, respectively, with the peaks at lower binding energy (795.2 eV and 780.1 eV) attributed to Co^{3+}, and the peaks at higher binding energy (796.7 eV and 781.5 eV) assigned to Co^{2+} [33,36,46]. The ratio of Co^{3+}/Co^{2+} was calculated by peak area and shown in Fig. 3a. It is noted that the Co^{3+}/Co^{2+} ratio of 1.22 %Na-Co_3O_4 was much higher than samples with lower Na content, which was in accordance with the phenomenon in recent research that alkali metal may occupy the tetrahedral site of Co_3O_4 and generate excess Co^{3+} [36,47]. After reaction, as shown in Fig. 3b and Fig. S5b, weak peaks of Co^0 appeared over all the samples (around 778.2 eV) [48–50], which was in accordance with XRD results. It was interesting that after reaction, the Co^{3+}/Co^{2+} ratio of used 1.22 %Na-Co_3O_4 was lower than 0.88 %Na-Co_3O_4 and 0.77 %Na-Co_3O_4, which was possibly due to the stronger reducibility and better interaction with NH_3.

The O 1 s XPS spectra of fresh 1.22 %Na-Co_3O_4, 0.88 %Na-Co_3O_4, and 0.77 %Na-Co_3O_4 are shown in Fig. 3c, in which each spectrum has been deconvoluted into three peaks, including chemisorbed oxygen (denoted as O_A thereafter) at around 530.8 eV, lattice oxygen (denoted

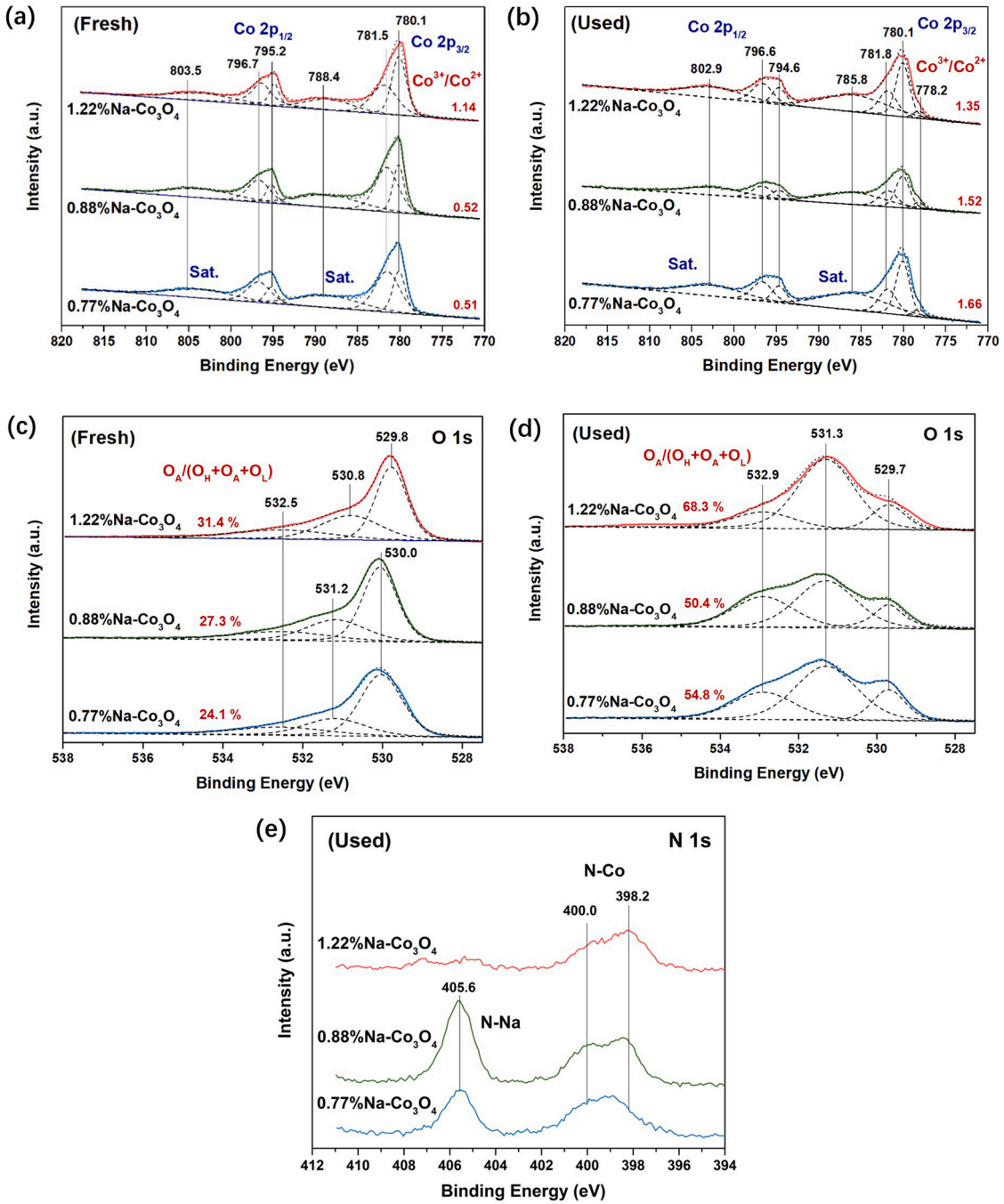

Fig. 3. XPS spectra of (a, b) Co 2p, (c, d) O 1 s over fresh and used 1.22 %Na-Co_3O_4, 0.88 %Na-Co_3O_4, and 0.77 %Na-Co_3O_4, and (e) N 1 s over used samples.

as O_L) at around 529.8 eV, and surface hydroxyl groups (denoted as O_H) at around 532.5 eV, respectively [33,51]. By calculating and comparing the $O_A/(O_H+O_A+O_L)$ ratio, it was found that the proportion of O_A decreased in the sequence of 1.22 %Na-Co_3O_4 > 0.88 %Na-Co_3O_4 > 0.77 %Na-Co_3O_4, which was on account of weakly-adsorbed oxygen anions induced by Na [36]. As O_A is adsorbed on oxygen defects, the result further confirmed the largest amount of oxygen vacancies on 1.22 %Na-Co_3O_4, which may accelerate cracking of NH_3 [18,52,53]. According to literatures, Co^{3+} is related to the formation of oxygen vacancies due to the weak bonding with lattice oxygen [33,46]. Therefore, the largest amount of oxygen vacancies agreed well with higher Co^{3+}/Co^{2+} ratio over 1.22 %Na-Co_3O_4. After reaction, the peak intensity of O_L decreased obviously (Fig. 3d), due to the reduction by NH_3. In addition, the O_A proportion of used 1.22 %Na-Co_3O_4 was still higher than other two samples, indicating more oxygen vacancies after reaction. The higher surface Co^{3+}/Co^{2+} ratio, accompanied with more oxygen vacancies over 1.22 %Na-Co_3O_4, was related to the stronger reducibility of Co as revealed by H_2-TPR results in Fig. 2d.

During the reaction in NH_3 atmosphere, N may be introduced on the surface of samples. Therefore, the N 1 s XPS experiments of used samples were conducted additionally with results shown in Fig. 3e and Fig. S6. Interestingly, as for 0.88 %Na-Co_3O_4 and 0.77 %Na-Co_3O_4, the peaks at 405.6 eV were ascribed to N-Na while the peaks around 400.0 eV and 398.2 eV were assigned to N-Co [54–58]. However, only N-Co peaks were observed over 1.22 %Na-Co_3O_4. This revealed that Na ions were in more stable chemical state, and in turn confirmed the stronger interaction between Co and NH_3 during the reaction over 1.22 %Na-Co_3O_4. Such strong interaction was possibly related to the modified reducibility

of Co and agreed well with XRD results of used samples, in which used 1.22 %Na-Co_3O_4 showed the strongest peak intensity of Co^0.

The proportion of surface atoms were also measured by XPS experiments. It is interesting that the surface Na content of 1.22 %Na-Co_3O_4 was obviously higher than bulk phase, indicating more Na concentrated on the surface. The surface Na content of fresh samples decreased in the sequence of Na-Co_3O_4-unwashed > 1.22 %Na-Co_3O_4 > 0.88 %Na-Co_3O_4 > 0.77 %Na-Co_3O_4 (as shown in Table S4), which was in accordance with the results of bulk contents tested by ICP-OES. This is further confirmed by Na 1 s XPS spectra with peaks around 1071.8 eV in Fig. S7, in which the peak intensity increased with high Na content [33]. It is also observed that both for fresh and used catalysts, the peaks of Na 1 s of 1.22 %Na-Co_3O_4 shifted to lower binding energy compared with other two samples, which further verified the electron transfer from Na. In addition, the surface Na contents of used samples were higher than that of fresh samples, respectively, indicating surface concentration of Na during pretreatment and reaction (Table S4), which magnified the effect of Na on the catalytic activity.

As the adsorption of NH_3 was the first step in NH_3 decomposition reaction, the surface acidity was evaluated by NH_3-TPD studies with results shown in Fig. 4a. A broad peak with strong intensity around 230 °C was observed over Na-Co_3O_4-unwashed. As for other Na-doped samples, broad desorption peaks above 100 °C were observed, with much weaker intensity compared with Na-Co_3O_4-unwashed. In contrast, Co_3O_4-CA showed a weak peak between 300 °C and 400 °C. This clearly revealed that Na produced more weak acid sites over Co_3O_4, which benefited the adsorption of NH_3 at low temperature. To further identify the adsorbed ammonia species, in-situ DRIFT analysis of adsorbed NH_3 after Ar purging at 200 °C were conducted and shown in Fig. 4b. The bands around 1598 and 1274 cm^{-1} were attributed to NH_3 coordinated with Lewis acid sites and the bands at 1683 and 1466 cm^{-1} were assigned to NH_4^+ coordinated with Brønsted acid sites [59–61]. It is observed that the peak intensity of both Lewis and Brønsted acid sites over 1.22 %Na-Co_3O_4 was slightly stronger than other Na-doped samples, indicating more adsorbed ammonia species at 200 °C. Combined with NH_3-TPD results, it is speculated that Na generated more weak acid sites over 1.22 %Na-Co_3O_4, thus adsorbed more NH_3 at low temperature. In addition, as for Na-Co_3O_4-unwashed and 1.22 %Na-Co_3O_4, the bands at 1526 cm^{-1} were due to amide (-NH_2) scissoring or wagging [53,61], indicating that part of adsorbed NH_3 was activated at 200 °C. As for samples with lower Na content (0.88 %Na-Co_3O_4 and 0.77 %Na-Co_3O_4), no bands of -NH_2 was observed at the same temperature, which indicated that Na also benefited the dehydrogenation of NH_3 at low temperature.

It was recognized that basicity is related to the desorption of products for NH_3 cracking [11]. As a result, CO_2-TPD studies were conducted to evaluate the surface basicity of prepared samples, with results shown in Fig. 4c. It was noted that Co_3O_4-CA hardly showed desorption peak, which was probably due to its low specific surface area. For Na-doped samples, the CO_2 desorption peaks gradually appeared with increasing Na content. It can be concluded that Na generated more basic sites over Co_3O_4, which was due to its strong electron donating ability. As for Na-Co_3O_4-unwashed, desorption peaks around 165 °C, 452 °C, and 540 °C appeared, which were ascribed to the CO_2 desorbed from weak basic sites, medium basic sites, and strong basic sites, respectively [38, 62–65]. In contrast, the CO_2 desorption peaks of 1.22 %Na-Co_3O_4 were below 400 °C, indicating only weak and medium basic sites over the sample. To monitor the desorption of products during the NH_3 decomposition reaction, NH_3-TPSR experiments were conducted by SVUV-PIMS with high sensitivity during the temperature-rise period,

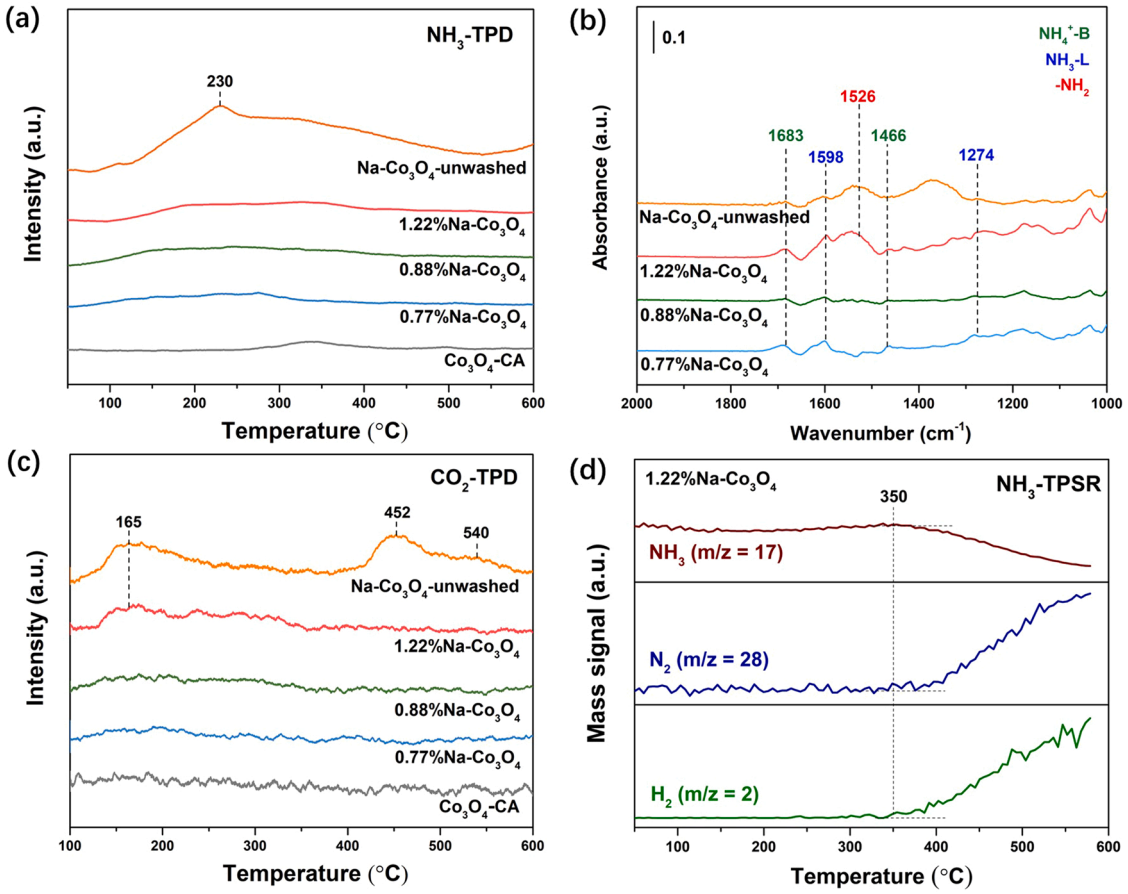

Fig. 4. (a) NH_3-TPD results over Na-doped Co_3O_4 catalysts and Co_3O_4-CA, (b) In-situ DRIFT spectra of adsorbed NH_3 species (after NH_3 adsorption and Ar purging) over Na-doped Co_3O_4 catalysts at 200 °C, (c) CO_2-TPD results over Na-doped Co_3O_4 catalysts and Co_3O_4-CA, and (d) NH_3-TPSR results over 1.22 %Na-Co_3O_4.

with the detection of NH_3 ($m/z = 17$), hydrogen ($m/z = 2$), and nitrogen ($m/z = 28$). The results in Fig. 4d showed that the NH_3 decomposition reaction over 1.22 %Na-Co_3O_4 started at around 350 °C. Furthermore, the desorption of N_2 and H_2 was observed simultaneously with the decrease of NH_3, indicating the immediate desorption of products. Combined with CO_2-TPD results, as no strong basic site was observed over 1.22 %Na-Co_3O_4 above 350 °C, it is speculated that surface basicity, as well as the desorption of products, is not decisive for the improved activity in this research. Instead, the improved acidity and promoted dehydrogenation of NH_3 played a more crucial role.

To further explore the reactivity of adsorbed ammonia species during reaction, in-situ DRIFT analysis was also conducted. As shown in Fig. 5, the peaks at 1626 and 1120 cm^{-1} ascribed to gaseous-phase NH_3 and/or physically adsorbed NH_3 over each sample [25]. The bands around 1598, 1326, 1274 and 1033 cm^{-1} were owing to NH_3 coordinated with Lewis acid sites and the bands at 1683 and 1466 cm^{-1} were ascribed to NH_4^+ coordinated with Brønsted acid sites [59–61,66–68], respectively. Besides, the bands at 1526, 1349, and 1140 cm^{-1} were due to -NH_2 species [53,59,61,69,70]. It was observed that with the increase in temperature from 200 °C to 400 °C, the band due to -NH_2 species at 1526 cm^{-1} over Na-Co_3O_4-unwashed increased markedly. Similarly, as for 1.22 %Na-Co_3O_4, the intensity of bands due to -NH_2 species (1526 cm^{-1}) increased with the temperature elevating from 200 °C to 300 °C. However, interestingly, when the temperature further rising to 400 °C, the band of -NH_2 species became weaker, which was possibly due to further reaction as the NH_3 decomposition started at around 350 °C (from NH_3-TPSR results in Fig. 4d). For 0.88 %Na-Co_3O_4 and 0.77 %Na-Co_3O_4, the bands due to -NH_2 species appeared above 300 °C were weaker compared with the former two samples. The result further validated that the ammonia species were activated more easily and took part into the reaction at lower temperature over 1.22 %Na-Co_3O_4.

Overall, as revealed by DRIFT studies, the -NH_2 species over Na-Co_3O_4-unwashed was hard to be further cracked, which was possibly due to the weaker reducibility of Co species. Theoretical calculation predicted that the rate-determining step to be the removal of the second hydrogen from -NH_2 for Co [71]. This may explain the lower NH_3 decomposition activity of Na-Co_3O_4-unwashed compared with 1.22 % Na-Co_3O_4. Although the rate-determination step over Co-based catalysts was under debate [17,49,71], it is widely accepted that the binding with N was the key factor in the process of cracking NH_3 [49,72]. Extensive investigations, including experiments as well as theoretical calculations, showed that Co possessed relative weak combination with N [71–76]. In our study, the enhanced interaction with NH_3 due to the strong reducibility of Co, along with the promoted NH_3 dehydrogenation, accounted for the higher activity over 1.22 %Na-Co_3O_4.

Furthermore, K-doped Co_3O_4 catalysts were prepared in the same way (except that the precipitant was replaced by KOH), with results of NH_3 decomposition activity shown in Fig. S8. The NH_3 decomposition activity decreased in the sequence of 0.42 %K-Co_3O_4 > 0.04 %K-Co_3O_4 > 0.02 %K-Co_3O_4, which was in the same way as Na-doped samples. This implied that the influence of K on the catalytic performance of Co_3O_4 for NH_3 decomposition was possibly similar to Na. Owing to the larger radius of K, it is reasonable that K-doped samples exhibited higher NH_3 decomposition activity than Na-doped ones. Additionally, 0.42 %K-Co_3O_4 showed higher NH_3 cracking performance than supported 20 % Co/CeO_2, and good long-term stability with NH_3 conversion above 70 % up to 100 h at 500 °C (as shown in Fig. S9). As the preparation method of alkali-doped Co_3O_4 is simple, it also provides a common and easy

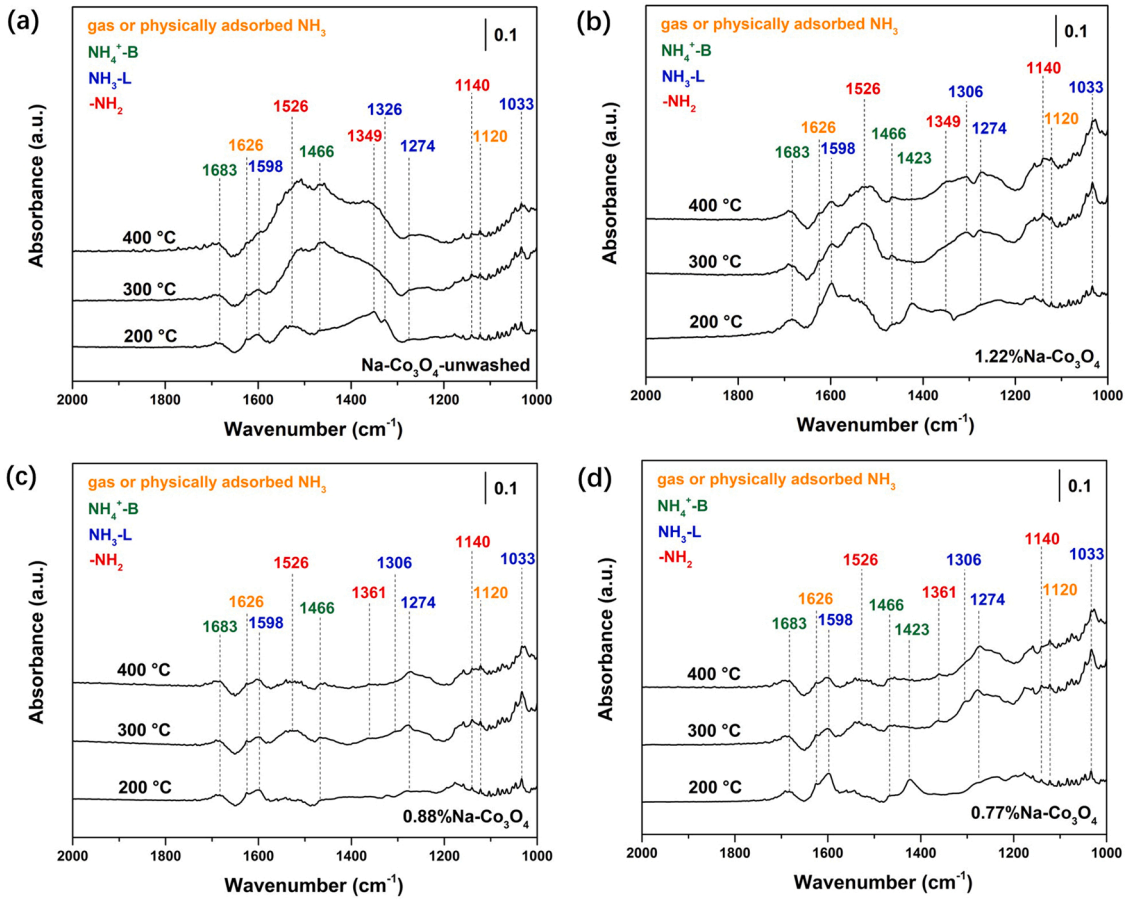

Fig. 5. In-situ DRIFT spectra of NH_3 species over (a) Na-Co_3O_4-unwashed, (b) 1.22 %Na-Co_3O_4, (c) 0.88 %Na-Co_3O_4, and (d) 0.77 %Na-Co_3O_4 in 1 % NH_3/Ar at elevated temperature.

strategy in the practical design and use of cobalt-based catalysts for NH_3 decomposition.

4. Conclusion

In summary, it was found that the NH_3 decomposition activity of Co_3O_4 was improved by doping alkali metals. Characterizations showed that appropriate amount of Na partly inserted into the lattice of Co_3O_4, weakened the Co-O coordination, and thus enhanced the reducibility of fresh sample. Owing to more reducible Co^{3+}, strong interaction with NH_3 was induced over 1.22 %Na-Co_3O_4 during reaction. Moreover, appropriate content of Na generated more weak acid sites and facilitated the adsorption and activation of NH_3 at low temperature. Therefore, the dehydrogenation of surface intermediate (-NH_2 species) was accelerated and the intrinsic activity for NH_3 decomposition was enhanced. This universal method could be extended to fabricate cobalt-based catalysts for the potential application of NH_3 as H_2 carrier.

CRediT authorship contribution statement

Wenshuo Zhang: Methodology, Formal analysis, Investigation, Writing - original draft. **Weili Zhou:** Software, Validation. **Yangfeng Li:** Investigation, Writing - review & editing. **Jie Ren:** Writing - review & editing. **Zhandong Wang:** Supervision, Funding acquisition.

Declaration of Competing Interest

The authors declare that they have no known competing financial interests or personal relationships that could have appeared to influence the work reported in this paper.

Data availability

Data will be made available on request.

Acknowledgments

This work was supported by the DNL Cooperation Fund, CAS (DNL202005) and by National Key Research and Development Program of China (2019YFA0405602).

Appendix A. Supporting information

Supplementary data associated with this article can be found in the online version at doi:10.1016/j.apcatb.2023.122644.

References

[1] S. Wu, N. Salmon, M. Li, R. Bañares-Alcántara, S. Tsang, Energy decarbonization via green H_2 or NH_3? ACS Energy Lett. (2022) 1021–1033, https://doi.org/10.1021/acsenergylett.1c02816.

[2] H. Fang, D. Liu, Y. Luo, Y. Zhou, S. Liang, X. Wang, B. Lin, L. Jiang, Challenges and opportunities of Ru-based catalysts toward the synthesis and utilization of ammonia, ACS Catal. 12 (2022) 3938–3954, https://doi.org/10.1021/acscatal.2c00090.

[3] R. Service, Liquid sunshine, Science 361 (2018) 120–123, https://doi.org/10.1126/science.361.6398.120.

[4] N. Morlanés, S. Katikaneni, S. Paglieri, A. Harale, B. Solami, S. Sarathy, J. Gascon, A technological roadmap to the ammonia energy economy: current state and missing technologies, Chem. Eng. J. 408 (2021), 127310, https://doi.org/10.1016/j.cej.2020.127310.

[5] Y. Yuan, L. Zhou, H. Robatjazi, J. Bao, J. Zhou, A. Bayles, L. Yuan, M. Lou, M. Lou, S. Khatiwada, E. Carter, P. Nordlander, N. Halas, Earth-abundant photocatalyst for H_2 generation from NH_3 with light-emitting diode illumination, Science 378 (2022) 889–893, https://doi.org/10.1126/science.abn5636.

[6] S. Giddey, S. Badwal, C. Munnings, M. Dolan, Ammonia as a renewable energy transportation media, ACS Sustain. Chem. Eng. 5 (2017) 10231–10239, https://doi.org/10.1021/acssuschemeng.7b02219.

[7] A. Valera-Medina, H. Xiao, M. Owen-Jones, W. David, P. Bowen, Ammonia for power, Prog. Energ. Combust. 69 (2018) 63–102, https://doi.org/10.1016/j.pecs.2018.07.001.

[8] D. MacFarlane, P. Cherepanov, J. Choi, B. Suryanto, R. Hodgetts, J. Bakker, F. Vallana, A. Simonov, A roadmap to the ammonia economy, Joule 4 (2020) 1186–1205, https://doi.org/10.1016/j.joule.2020.04.004.

[9] A. Hill, L. Torrente-Murciano, Low temperature H_2 production from ammonia using ruthenium-based catalysts: Synergetic effect of promoter and support, Appl. Catal. B 172–173 (2015) 129–135, https://doi.org/10.1016/j.apcatb.2015.02.011.

[10] K. Nagaoka, T. Eboshi, Y. Takeishi, R. Tasaki, K. Honda, K. Imamura, K. Sato, Carbon-free H_2 production from ammonia triggered at room temperature with an acidic RuO_2/γ-Al_2O_3 catalyst, Sci. Adv. 3 (2017), e1602747, https://doi.org/10.1126/sciadv.1602747.

[11] S. Mukherjee, S. Devaguptapu, A. Sviripa, C. Lund, G. Wu, Low-temperature ammonia decomposition catalysts for hydrogen generation, Appl. Catal. B 226 (2018) 162–181, https://doi.org/10.1016/j.apcatb.2017.12.039.

[12] X. Hu, X. Fu, W. Wang, X. Wang, K. Wu, R. Si, C. Ma, C. Jia, C. Yan, Ceria-supported ruthenium clusters transforming from isolated single atoms for hydrogen production via decomposition of ammonia, Appl. Catal. B 268 (2020), 118424, https://doi.org/10.1016/j.apcatb.2019.118424.

[13] C. Chen, K. Wu, H. Ren, C. Zhou, Y. Luo, L. Lin, C. Au, L. Jiang, Ru-based catalysts for ammonia decomposition: a mini-review, Energ. Fuels 35 (2021) 11693–11706, https://doi.org/10.1021/acs.energyfuels.1c01261.

[14] X. Duan, G. Qian, X. Zhou, D. Chen, W. Yuan, MCM-41 supported Co-Mo bimetallic catalysts for enhanced hydrogen production by ammonia decomposition, Chem. Eng. J. 207–208 (2012) 103–108, https://doi.org/10.1016/j.cej.2012.05.100.

[15] P. Yu, H. Wu, J. Guo, P. Wang, F. Chang, W. Gao, W. Zhang, L. Liu, P. Chen, Effect of BaNH, CaNH, Mg_3N_2 on the activity of Co in NH_3 decomposition catalysis, J. Energy Chem. 46 (2020) 16–21, https://doi.org/10.1016/j.jechem.2019.10.014.

[16] K. Kirste, K. McAulay, T. Bell, D. Stoian, S. Laassiri, A. Daisley, J. Hargreaves, K. Mathisen, L. Torrente-Murciano, COx-free hydrogen production from ammonia-mimicking the activity of Ru catalysts with unsupported Co-Re alloys, Appl. Catal. B 280 (2021), 119405, https://doi.org/10.1016/j.apcatb.2020.119405.

[17] H. Tabassum, S. Mukherjee, J. Chen, D. Holiharimanana, S. Karakalos, X. Yang, S. Hwang, T. Zhang, B. Lu, M. Chen, Z. Tang, E. Kyriakidou, Q. Ge, G. Wu, Hydrogen generation via ammonia decomposition on highly efficient and stable Ru-free catalysts: approaching complete conversion at 450 °C, Energy Environ. Sci. 15 (2022) 4190–4200, https://doi.org/10.1039/d1ee03730g.

[18] C. Huang, Y. Yu, X. Tang, Z. Liu, J. Zhang, C. Ye, Y. Ye, R. Zhang, Hydrogen generation by ammonia decomposition over Co/CeO_2 catalyst: influence of support morphologies, Appl. Surf. Sci. 532 (2020), 147335, https://doi.org/10.1016/j.apsusc.2020.147335.

[19] T. Bell, H. Ménard, J. González Carballo, R. Tooze, L. Torrente-Murciano, Hydrogen production from ammonia decomposition using Co/γ-Al2O3 catalysts-Insights into the effect of synthetic method, Int. J. Hydrog. Energy 45 (2020) 27210–27220, https://doi.org/10.1016/j.ijhydene.2020.07.090.

[20] G. Li, X. Yu, F. Yin, Z. Lei, H. Zhang, X. He, Production of hydrogen by ammonia decomposition over supported Co_3O_4 catalysts, Catal. Today 402 (2022) 45–51, https://doi.org/10.1016/j.cattod.2022.02.020.

[21] C. Huang, H. Li, J. Yang, C. Wang, F. Hu, X. Wang, Z. Lu, G. Feng, R. Zhang, $Ce_{0.6}Zr_{0.3}Y_{0.1}O_2$ solid solutions-supported Ni-Co bimetal nanocatalysts for NH_3 decomposition, Appl. Surf. Sci. 478 (2019) 708–716, https://doi.org/10.1016/j.apsusc.2019.01.269.

[22] M. Pinzón, A. Romero, A. de Lucas-Consuegra, A. de la Osa, P. Sánchez, COx-free hydrogen production from ammonia at low temperature using Co/SiC catalyst: effect of promoter, Catal. Today 390- 391 (2022) 34–47, https://doi.org/10.1016/j.cattod.2021.12.005.

[23] D. Varisli, N. Kaykac, COx free hydrogen production over cobalt incorporated silicate structured mesoporous catalysts, Appl. Catal. B 127 (2012) 389–398, https://doi.org/10.1016/j.apcatb.2012.08.042.

[24] A. Srifa, K. Okura, T. Okanishi, H. Muroyama, T. Matsui, K. Eguchi, Hydrogen production by ammonia decomposition over Cs-modified Co_3Mo_3N catalysts, Appl. Catal. B 218 (2017) 1–8, https://doi.org/10.1016/j.apcatb.2017.06.034.

[25] J. Cha, T. Lee, Y. Lee, H. Jeong, Y. Jo, Y. Kim, S. Nam, J. Han, K. Lee, C. Yoon, H. Sohn, Highly monodisperse sub-nanometer and nanometer Ru particles confined in alkali-exchanged zeolite Y for ammonia decomposition, Appl. Catal. B 283 (2021), 119627, https://doi.org/10.1016/j.apcatb.2020.119627.

[26] Y. Gu, X. Fu, P. Du, D. Gu, Z. Jin, Y. Huang, R. Si, L. Zheng, Q. Song, C. Jia, C. Weidenthaler, In situ X-ray diffraction study of Co-Al nanocomposites as catalysts for ammonia decomposition, J. Phys. Chem. C. 119 (2015) 17102–17110, https://doi.org/10.1021/acs.jpcc.5b02932.

[27] X. Hu, W. Wang, Y. Gu, Z. Jin, Q. Song, C. Jia, $Co-SiO_2$ nanocomposite catalysts for COx-free hydrogen production by ammonia decomposition, ChemPlusChem 82 (2017) 368–375, https://doi.org/10.1002/cplu.201600444.

[28] X. Duan, J. Ji, X. Yan, G. Qian, D. Chen, X. Zhou, Understanding Co-Mo catalyzed ammonia decomposition: Influence of calcination atmosphere and identification of active phase, ChemCatChem 8 (2016) 938–945, https://doi.org/10.1002/cctc.201501275.

[29] Ł. Czekajło, Z. Lendzion-Bieluń, Effect of preparation conditions and promoters on the structure and activity of the ammonia decomposition reaction catalyst based on nanocrystalline cobalt, Chem. Eng. J. 289 (2016) 254–260, https://doi.org/10.1016/j.cej.2015.12.093.

[30] L. Huo, B. Liu, H. Li, B. Cao, X. Hu, X. Fu, C. Jia, J. Zhang, Component synergy and armor protection induced superior catalytic activity and stability of ultrathin Co-Fe spinel nanosheets confined in mesoporous silica shells for ammonia decomposition reaction, Appl. Catal. B 253 (2019) 121–130, https://doi.org/10.1016/j.apcatb.2019.04.053.

[31] C. Wu, Z. Jin, K. Xu, W. Wang, C. Jia, $Co_aSm_bO_x$ Catalyst with excellent catalytic performance for NH_3 decomposition, Chin. J. Chem. 39 (2021) 2359–2366, https://doi.org/10.1002/cjoc.202100176.

[32] M. Sun, L. Wang, B. Feng, Z. Zhang, G. Lu, Y. Guo, The role of potassium in K/Co_3O_4 for soot combustion under loose contact, Catal. Today 175 (2011) 100–105, https://doi.org/10.1016/j.cattod.2011.04.044.

[33] W. Dai, M. Zou, C. Zhao, J. Zhang, L. Wang, X. Wang, L. Yang, L. Zhou, J. Zou, X. Luo, S. Luo, G. Jing, Monoatomic oxygen fueled by oxygen vacancies governs the photothermocatalytic deep oxidation of toluene on Na-doped Co_3O_4, Appl. Catal. B 317 (2022), 121769, https://doi.org/10.1016/j.apcatb.2022.121769.

[34] L. Zhang, M. Li, T. Ren, X. Liu, Z. Yuan, Ce-modified Ni nanoparticles encapsulated in SiO_2 for CO-free hydrogen production via ammonia decomposition, Int. J. Hydrogen Energy 40 (2015) 2648–2656, https://doi.org/10.1016/j.ijhydene.2014.12.079.

[35] K. Asano, C. Ohnishi, S. Iwamoto, Y. Shioya, M. Inoue, Potassium-doped Co_3O_4 catalyst for direct decomposition of N_2O, Appl. Catal. B 78 (2008) 242–249, https://doi.org/10.1016/j.apcatb.2007.09.016.

[36] W. Zhu, X. Wang, C. Li, X. Chen, W. Li, Z. Liu, C. Liang, Defect engineering over Co_3O_4 catalyst for surface lattice oxygen activation and boosted propane total oxidation, J. Catal. 413 (2022) 150–162, https://doi.org/10.1016/j.jcat.2022.06.024.

[37] Z. Zhang, H. Ai, M. Fu, Y. Hu, J. Liu, Y. Ji, V. Vasanthakumar, B. Yuan, A new insight into catalytic ozonation of ammonia by MgO/Co_3O_4 composite: the effects, reaction kinetics and mechanism, Chem. Eng. J. 418 (2021), 129461, https://doi.org/10.1016/j.cej.2021.129461.

[38] Y. Jian, M. Tian, C. He, J. Xiong, Z. Jiang, H. Jin, L. Zheng, R. Albilali, J. Shi, Efficient propane low-temperature destruction by Co_3O_4 crystal facets engineering: unveiling the decisive role of lattice and oxygen defects and surface acid-base pairs, Appl. Catal. B 283 (2021), 119657, https://doi.org/10.1016/j.apcatb.2020.119657.

[39] X. Wang, Y. Liu, T. Zhang, Y. Luo, Z. Lan, K. Zhang, J. Zuo, L. Jiang, R. Wang, Geometrical-site-dependent catalytic activity of ordered mesoporous Co-based spinel for benzene oxidation: In situ DRIFTS study coupled with Raman and XAFS spectroscopy, ACS Catal. 7 (2017) 1626–1636, https://doi.org/10.1021/acscatal.6b03547.

[40] T. Wu, S. Sun, J. Song, S. Xi, Y. Du, B. Chen, W.A. Sasangka, H. Liao, C.L. Gan, G. G. Scherer, L. Zeng, H. Wang, H. Li, A. Grimaud, Z.J. Xu, Iron-facilitated dynamic active-site generation on spinel $CoAl_2O_4$ with self-termination of surface reconstruction for water oxidation, Nat. Catal. 2 (2019) 763–772, https://doi.org/10.1038/s41929-019-0325-4.

[41] H. Liu, S. Yang, G. Wang, H. Liu, Y. Peng, C. Sun, J. Li, J. Chen, Strong electronic orbit coupling between cobalt and single-atom praseodymium for boosted nitrous oxide decomposition on Co_3O_4 catalyst, Environ. Sci. Technol. 56 (2022) 16325–16335, https://doi.org/10.1021/acs.est.2c06677.

[42] Y. Lu, T. Liu, C.L. Dong, C. Yang, L. Zhou, Y.C. Huang, Y. Li, B. Zhou, Y. Zou, S. Wang, Tailoring competitive adsorption sites by oxygen-vacancy on cobalt oxides to enhance the electrooxidation of biomass, Adv. Mater. 34 (2022), e2107185, https://doi.org/10.1002/adma.202107185.

[43] W. Zhang, K. Lassen, C. Descorme, J. Valverde, A. Giroir-Fendler, Effect of the precipitation pH on the characteristics and performance of Co_3O_4 catalysts in the total oxidation of toluene and propane, Appl. Catal. B-Environ. 282 (2021), 119566, https://doi.org/10.1016/j.apcatb.2020.119566.

[44] S. Huang, L. Yang, G. Xu, T. Wei, J. Tian, X. Liu, H. Li, Z. Xiang, J. Cao, X. Wei, Hollow Co_3O_4@N-doped carbon nanocrystals anchored on carbon nanotubes for freestanding anode with superior Li/Na storage performance, Chem. Eng. J. 415 (2021), 128861, https://doi.org/10.1016/j.cej.2021.128861.

[45] Y. Gu, D. Xu, Y. Huang, Z. Long, G. Chen, COx-free hydrogen production via ammonia decomposition over mesoporous Co/Al_2O_3 catalysts with highly dispersed Co species synthesized by a facile method, Dalton Trans. 50 (2021) 1443–1452, https://doi.org/10.1039/d0dt03262j.

[46] Y. Ma, L. Wang, J. Ma, H. Wang, C. Zhang, H. Deng, H. He, Investigation into the enhanced catalytic oxidation of o-xylene over MOF-derived Co_3O_4 with different shapes: the role of surface twofold-coordinate lattice oxygen (O_{2f}), ACS Catal. 11 (2021) 6614–6625, https://doi.org/10.1021/acscatal.1c01116.

[47] L.T. Anh, A.K. Rai, T.V. Thi, J. Gim, S. Kim, V. Mathew, J. Kim, Enhanced electrochemical performance of novel K-doped Co_3O_4 as the anode material for secondary lithium-ion batteries, J. Mater. Chem. A 2 (2014) 6966–6975, https://doi.org/10.1039/c4ta00532e.

[48] L. Li, R. Jiang, W. Chu, H. Cang, H. Chen, J. Yan, Cobalt nanoparticles embedded in a porous carbon matrix as an efficient catalyst for ammonia decomposition, Catal. Sci. Technol. 7 (2017) 1363–1371, https://doi.org/10.1039/c7cy00086c.

[49] G. Li, H. Zhang, X. Yu, Z. Lei, F. Yin, X. He, Highly efficient Co/NC catalyst derived from ZIF-67 for hydrogen generation through ammonia decomposition, Int. J. Hydrogen Energy 47 (2022) 12882–12892, https://doi.org/10.1016/j.ijhydene.2022.02.046.

[50] Q. Yao, Z. Lu, Y. Wang, X. Chen, G. Feng, Synergetic catalysis of non-noble bimetallic Cu-Co nanoparticles embedded in SiO_2 nanospheres in hydrolytic dehydrogenation of ammonia borane, J. Phys. Chem. C. 119 (2015) 14167–14174, https://doi.org/10.1021/acs.jpcc.5b02403.

[51] S. Guo, H. Wang, W. Yang, H. Fida, L. You, K. Zhou, Scalable synthesis of Ca-doped α-Fe_2O_3 with abundant oxygen vacancies for enhanced degradation of organic pollutants through peroxymonosulfate activation, Appl. Catal. B 262 (2020), 118250, https://doi.org/10.1016/j.apcatb.2019.118250.

[52] K. Wu, C. Cao, C. Zhou, Y. Luo, C. Chen, L. Lin, C. Au, L. Jiang, Engineering of Ce^{3+}-O-Ni structures enriched with oxygen vacancies via Zr doping for effective generation of hydrogen from ammonia, Chem. Eng. Sci. 245 (2021), 116818, https://doi.org/10.1016/j.ces.2021.116818.

[53] Q. Do, Y. Kim, T. Le, G. Kim, J. Kim, T. Kim, Y. Lee, H. Chae, Facile one-pot synthesis of Ni-based catalysts by cation-anion double hydrolysis method as highly active Ru-free catalysts for green H_2 production via NH_3 decomposition, Appl. Catal. B 307 (2022), 121167, https://doi.org/10.1016/j.apcatb.2022.121167.

[54] Y. Yang, R. Zeng, Y. Xiong, F.J. DiSalvo, H.D. Abruna, Cobalt-based nitride-core oxide-shell oxygen reduction electrocatalysts, J. Am. Chem. Soc. 141 (2019) 19241–19245, https://doi.org/10.1021/jacs.9b10809.

[55] T. Zhang, J. Bian, Y. Zhu, C. Sun, FeCo nanoparticles encapsulated in N-doped carbon nanotubes coupled with layered double (Co, Fe) hydroxide as an efficient bifunctional catalyst for rechargeable zinc-air batteries, Small (2021), e2103737, https://doi.org/10.1002/smll.202103737.

[56] T. Zhang, F. Cheng, C. Zhao, H. Liu, X. Song, X. Li, W. Luo, Enriching atomic cobalt in an ultrathin porous carbon shell for enhanced electrocatalysis, ACS Appl. Mater. Interfaces 13 (2021) 52167–52173, https://doi.org/10.1021/acsami.1c10513.

[57] S. Guan, Y. Liu, H. Zhang, H. Wei, T. Liu, X. Wu, H. Wen, R. Shen, S. Mehdi, X. Ge, C. Wang, B. Liu, E. Liang, Y. Fan, B. Li, Atomic interface-exciting catalysis on cobalt nitride-oxide for accelerating hydrogen generation, Small 18 (2022), e2107417, https://doi.org/10.1002/smll.202107417.

[58] NIST X-ray Photoelectron Spectroscopy Database, NIST Standard Reference Database Number 20, National Institute of Standards and Technology, Gaithersburg MD 20899 (2000) doi:10.18434/T4T88K.

[59] W. Zhu, X. Tang, F. Gao, H. Yi, R. Zhang, J. Wang, C. Yang, S. Ni, The effect of non-selective oxidation on the $Mn_2Co_1O_x$ catalysts for NH_3-SCR: positive and non-positive, Chem. Eng. J. 385 (2020), 123797, https://doi.org/10.1016/j.cej.2019.123797.

[60] K. Zha, C. Feng, L. Han, H. Li, T. Yan, S. Kuboon, L. Shi, D. Zhang, Promotional effects of Fe on manganese oxide octahedral molecular sieves for alkali-resistant catalytic reduction of NOx: XAFS and in situ DRIFTs study, Chem. Eng. J. 381 (2020), 122764, https://doi.org/10.1016/j.cej.2019.122764.

[61] Y. Wang, W. Xu, C. Li, Y. Yang, Z. Geng, T. Zhu, Effects of IrO_2 nanoparticle sizes on Ir/Al_2O_3 catalysts for the selective catalytic oxidation of ammonia, Chem. Eng. J. 437 (2022), 135398, https://doi.org/10.1016/j.cej.2022.135398.

[62] Š. Hajduk, V.D.B.C. Dasireddy, B. Likozar, G. Dražić, Z.C. Orel, COx-free hydrogen production via decomposition of ammonia over Cu–Zn-based heterogeneous catalysts and their activity/stability, Appl. Catal. B 211 (2017) 57–67, https://doi.org/10.1016/j.apcatb.2017.04.031.

[63] S. Podila, H. Driss, S.F. Zaman, A.M. Ali, A.A. Al-Zahrani, M.A. Daous, L.A. Petrov, Effect of preparation methods on the catalyst performance of Co/Mg La mixed oxide catalyst for COx-free hydrogen production by ammonia decomposition, Int. J. Hydrog. Energy 42 (2017) 24213–24221, https://doi.org/10.1016/j.ijhydene.2017.07.112.

[64] S. Podila, H. Driss, S.F. Zaman, A.M. Ali, A.A. Al-Zahrani, M.A. Daous, L.A. Petrov, MgFe and Mg-Co-Fe mixed oxides derived from hydrotalcites: highly efficient catalysts for COx free hydrogen production from NH_3, Int. J. Hydrog. Energy 45 (2020) 873–890, https://doi.org/10.1016/j.ijhydene.2019.10.107.

[65] Z. Liu, X. Gao, B. Liu, W. Song, Q. Ma, T. Zhao, X. Wang, J.W. Bae, X. Zhang, J. Zhang, Highly stable and selective layered Co-Al-O catalysts for low-temperature CO_2 methanation, Appl. Catal. B 310 (2022), 121303, https://doi.org/10.1016/j.apcatb.2022.121303.

[66] F. Wang, G. He, B. Zhang, M. Chen, X. Chen, C. Zhang, H. He, Insights into the activation effect of H_2 pretreatment on Ag/Al_2O_3 catalyst for the selective oxidation of ammonia, ACS Catal. 9 (2019) 1437–1445, https://doi.org/10.1021/acscatal.8b03744.

[67] S. Chen, M.A. Vasiliades, Q. Yan, G. Yang, X. Du, C. Zhang, Y. Li, T. Zhu, Q. Wang, A.M. Efstathiou, Remarkable N_2-selectivity enhancement of practical NH_3-SCR over $Co_{0.5}Mn_1Fe_{0.25}Al_{0.75}O_x$-LDO: The role of Co investigated by transient kinetic and DFT mechanistic studies, Appl. Catal. B 277 (2020), 119186, https://doi.org/10.1016/j.apcatb.2020.119186.

[68] S. Li, W. Huang, H. Xu, T. Chen, Y. Ke, Z. Qu, N. Yan, Alkali-induced deactivation mechanism of V_2O_5-WO_3/TiO_2 catalyst during selective catalytic reduction of NO by NH_3 in aluminum hydrate calcining flue gas, Appl. Catal. B 270 (2020), 118872, https://doi.org/10.1016/j.apcatb.2020.118872.

[69] L. Ma, C.Y. Seo, M. Nahata, X. Chen, J. Li, J.W. Schwank, Shape dependence and sulfate promotion of CeO_2 for selective catalytic reduction of NOx with NH_3, Appl. Catal. B 232 (2018) 246–259, https://doi.org/10.1016/j.apcatb.2018.03.065.

[70] N. Zhang, L. Li, Y. Guo, J. He, R. Wu, L. Song, G. Zhang, J. Zhao, D. Wang, H. He, A MnO_2-based catalyst with H_2O resistance for NH_3-SCR: study of catalytic activity and reactants-H_2O competitive adsorption, Appl. Catal. B 270 (2020), 118860, https://doi.org/10.1016/j.apcatb.2020.118860.

[71] D.A. Hansgen, D.G. Vlachos, J.G. Chen, Using first principles to predict bimetallic catalysts for the ammonia decomposition reaction, Nat. Chem. 2 (2010) 484–489, https://doi.org/10.1038/nchem.626.

[72] C.J. Jacobsen, S. Dahl, B.S. Clausen, S. Bahn, A. Logadottir, J.K. Norskov, Catalyst design by interpolation in the periodic table: bimetallic ammonia synthesis catalysts, J. Am. Chem. Soc. 123 (2001) 8404–8405, https://doi.org/10.1021/ja010963d.

[73] A. Boisen, S. Dahl, J. Norskov, C. Christensen, Why the optimal ammonia synthesis catalyst is not the optimal ammonia decomposition catalyst, J. Catal. 230 (2005) 309–312, https://doi.org/10.1016/j.jcat.2004.12.013.

[74] W. Zheng, T.P. Cotter, P. Kaghazchi, T. Jacob, B. Frank, K. Schlichte, W. Zhang, D. S. Su, F. Schuth, R. Schlogl, Experimental and theoretical investigation of

molybdenum carbide and nitride as catalysts for ammonia decomposition, J. Am. Chem. Soc. 135 (2013) 3458–3464, https://doi.org/10.1021/ja309734u.
[75] W. Guo, D.G. Vlachos, Patched bimetallic surfaces are active catalysts for ammonia decomposition, Nat. Commun. 6 (2015) 8619, https://doi.org/10.1038/ncomms9619.
[76] L. Huo, X. Han, L. Zhang, B. Liu, R. Gao, B. Cao, W. Wang, C. Jia, K. Liu, J. Liu, J. Zhang, Spatial confinement and electron transfer moderating Mo-N bond strength for superior ammonia decomposition catalysis, Appl. Catal. B 294 (2021), 120254, https://doi.org/10.1016/j.apcatb.2021.120254.